Resonant Multi-Ion Conduction in a Simple Model of Calcium Channels

I. Kaufman*, R. Tindjong*, D. G. Luchinsky*†, P. V. E. McClintock*, R. S. Eisenberg‡,
*Department of Physics, Lancaster University, Lancaster LA1 4YB, Uk
Email: p.v.e.mcclintock@lancaster.ac.uk
†NASA Ames Research Center, MS 269-3, Moffett Field, CA, 94035, USA
‡Molecular Biophysics, Rush University, Chicago IL 60612, USA

***Abstract*—The ionic permeation of a biological ion channel is a multi-particle, non-equilibrium, stochastic process. Brownian dynamics simulations for a simple electrostatic model of the calcium channel reveal regular structure in the conductance and selectivity as functions of the negative fixed charge Q_f on the protein wall at the selectivity filter. This structure consists of distinct high conductance regions (conduction bands) separated by regions of near non-conductance (stop-bands). We demonstrate explicitly that the sharply-defined conduction/selectivity peak of the L-type calcium channel is attributable to the correlated motion of a pair of calcium ions that can occur when their mutual electrostatic repulsion balances their electrostatic attraction to the charge at the selectivity filter. We report self-consistent electrostatic calculations of single-file, double-ion, stochastic optimal trajectories, and of the energy profiles along these trajectories, for different Q_f. We show that the energy difference ΔE along the optimal path exhibits a pronounced minimum near $Q_f = 3e$ corresponding to an almost barrier-less ($\Delta E \sim k_B T$) resonance-like form of conduction. The electrostatics calculations agree well with the results of Brownian dynamics simulations. These results clarify the long-standing puzzle of how the L-type calcium channel exhibits, simultaneously, both high calcium selectivity and conduction at almost the rate of free diffusion.**

I. Introduction

The ionic permeation of a biological ion channel is a multi-particle, non-equilibrium, stochastic process. The permeating ion interacts with a thermal bath, with other permeating ions, and with fixed and induced charges on the protein walls [1]. The escape of an ion from a potential minimum within the channel can be perceived as a large fluctuation along an optimal stochastic trajectory [2].

Voltage-gated calcium channels, and the closely related sodium ion channels, are important for e.g. the transmission of action potentials, the control of muscle contraction, gene regulation, and neurotransmitter secretion. The effective function of calcium channels depends on their high selectivity for calcium Ca^{2+} ions as compared to monovalent sodium Na^+ ions. They exhibit the well-known anomalous mole fraction effect (AMFE), which is an effective blockade of Na^+ permeation by tiny concentrations of Ca^{2+}, combined with pA currents of Ca^{2+}. Despite their very similar structure, sodium channels exhibit the opposite kind of selectivity, favouring Na^+ over Ca^{2+} [3], [4].

The selectivity properties of a Ca^{2+} channel are determined by a narrow selectivity filter (SF) consisting of a strong binding site formed from protein residues whose net charge Q_f is negative. The most studied L-type calcium channel has 4-glutamate EEEE locus with $Q_f \sim 4e$ [4]. Although sodium channels are similar in structure to calcium channels, they have DEKA SF loci (and hence different $Q_f \sim 1e$), as well as different lengths and radii [3], [5].

Experimental studies of site-directed mutagenesis [6], [7] show that mutations changing the value of Q_f can convert a sodium-selective channel into calcium-selective channel and *vice versa*, but the underlying mechanisms of conduction and selectivity governing these transformations have remained unclear.

Based on parametric Brownian dynamics (BD) simulations of the current against Q_f in a simple calcium channel model, we have recently shown that the Ca^{2+} conduction and Ca^{2+}/Na^+ valence selectivity form a regular array of narrow conduction/selectivity bands as a function of Q_f separated by regions of non-conduction [8]. (One of these bands was simulated earlier by Corry [9].) These discrete bands relate to self-sustained, saturated Ca^{2+} conduction involving different numbers of ions.

We report below an investigation of the energetics of permeation for a generic electrostatic model of calcium-sodium channels. We calculate potential energy profiles along multi-ion, stochastic, optimal trajectories [2], [10] and show explicitly that there is a barrier-less conduction mechanism underlying the calcium and sodium conduction and selectivity bands.

II. Generic model of calcium channels

Our self-consistent electrostatic model of the channel represents its SF as a negatively-charged, axisymmetric, water-filled, cylinder in a protein hub spanning the cell membrane, as shown in Fig. 1. The negatively-charged protein residues are modeled as a rigid uniformly-charged ring around the SF carrying a net negative charge within the range $0 < Q_f < 6.5e$.

The smallest possible SF radius R of an L-type calcium channel has been shown to be $R = 2.8$ Å. Here, we use a value of $R = 3.0$ Å. The SF length was taken as $L = 12 - 16\mathring{A}$. The mobile sodium and calcium ions are treated as charged spheres of radius $R_i \approx 1$ Å (matching both ions), with diffusion coefficients $D_{Na} = 1.17 \times 10^{-9}$ m^2/s and $D_{Ca} = 0.79 \times 10^{-9}$ m^2/s, respectively.

We take both protein and water to be homogeneous continua with dielectric constants $\varepsilon_p = 2$ and $\varepsilon_w = 80$, respectively, together with an implicit model of ion hydration.

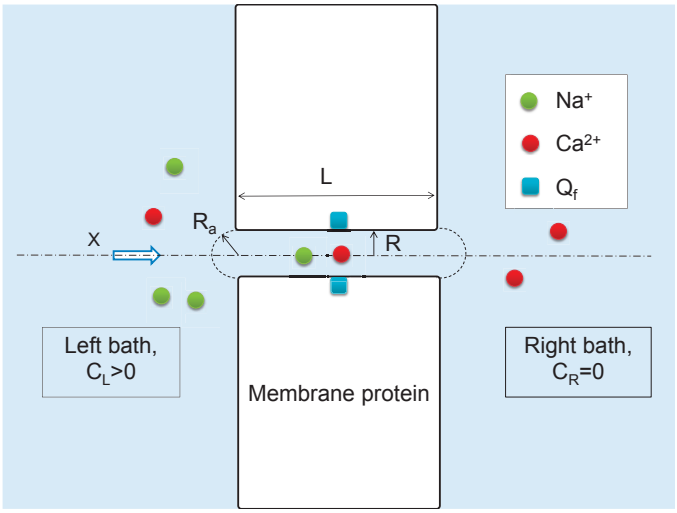

Fig. 1. Schematic diagram showing the generic model of the calcium ion channel. Its selectivity filter (SF) is modelled as an axisymmetric, water-filled, cylindrical hole of radius $R = 3$ Å and length $L = 12-16$ Å through the protein hub in the cellular membrane. There is a centrally-placed, homogeneous ring of negative charge $Q_f = 0 - 6.5e$. The left-hand bath (the extracellular space), contains Ca^{2+} or Na^{+} ions that are injected at the Smoluchowski diffusion rate at radius R_a. The domain length L_d=100 Å and its radius $R_d = 100$Å. The grid size is $h = 0.5$ Å. A potential difference of 0–75 mV is applied between the two baths.

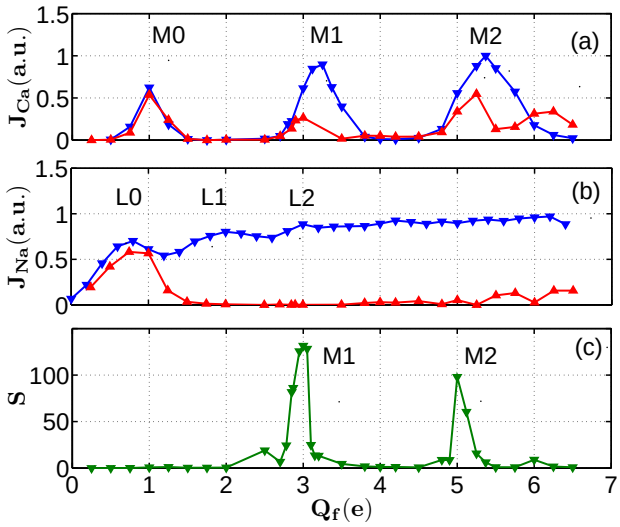

Fig. 2. The multi-ion conduction and selectivity bands for the model as determined by BD simulations (partly reworked from [8]). (a) Variation of the calcium current J_{Ca} with the fixed charge Q_f at the selectivity filter for pure (blue, point-down, triangles) and mixed baths (red, point-up, triangles). It exhibits clearly-resolved conduction bands M0, M1, and M2. (b) Variation of the sodium current J_{Na} with Q_f for pure (blue, point-down, triangles) and mixed (red, point-up, triangles) baths shows weakly-resolved, overlapping conduction bands L0, L1, L2. (c) The selectivity ratio $S = J_{Ca}/J_{Na}$ for the mixed salt shows little selectivity for small Q_f, but strong peaks corresponding to the M1 and M2 calcium bands.

The BD simulations were performed by the self-consistent, coupled, numerical solution of the 1D Langevin stochastic equation and the 3D axisymmetrical Poisson's equation. Our ion injection scheme connects the arrival rate j_{arr} to the bulk concentration C through the Smoluchowski diffusion rate: $j_{arr} = 2\pi DRC$ [11]. The model has been presented in details elsewhere, together with a discussion of its validity and limitations [8].

III. Discrete conduction and selectivity bands

Fig. 2 presents results from Brownian dynamics simulations of permeation for the generic channel model. Calcium J_{Ca} and sodium J_{Na} currents are plotted *vs.* Q_f for both a pure NaCl bath and for a mixed bath with Ca^{2+} and Na^{+} ions. Fig. 2(a) illustrates the regular structure that arises in J_{Ca} as a function of Q_f, showing the narrow conduction bands M0, M1, M2 separated by stop-bands of almost zero-conductance. Fig. 2(b) shows that in case of the pure bath, $J_{Na}(Q_f)$ exhibits weak local maxima that appear to be analogous to the calcium conduction bands shown in (a). We label them as L0, L1, L2, corresponding to their integer sodium occupancy $P_{Na} = 1, 2, 3$ of the SF. In mixed bath J_{Na} is blocked for $Q_f >= L1$. The selectivity ratio $S = J_{Ca}/J_{Na}$ plotted in Fig. 2(c) illustrates the strikingly resonant character of calcium selectivity in the M1 and M2 bands.

The bands obtained fall into an ordered sequence with increasing calcium selectivity: L0=0.5-0.7e (the sodium selective, non-blocking channel) $\rightarrow$ M0=1e (non-selective cation channel) $\rightarrow$ L1=1.5-2e (identified with the DEKA sodium channel) $\rightarrow$ M1=3e (identified with the L-type calcium channel) $\rightarrow$ M2=5e (identified with the RyR calcium channel) [8], [12].

IV. Resonant barrier-less conduction

Next, we consider the energetics of calcium and sodium conductivity in our model. We will show explicitly that there is a barrier-less permeation mechanism underlying the conduction and selectivity bands.

Fig. 3 shows how the almost barrier-less conductivity for the calcium single-ion M0 band appears as the consequence of a balance between Ca^{2+} ion self-repulsion and its attraction to the Q_f, and that it exhibits a resonance-like behaviour. Fig. 3(a) demonstrates the existence of an optimal (resonance) point Q_{opt} ($Q_{opt} = 0.87e$ for Ca^{2+} ions) where energy difference along S $\Delta E = |E_{max} - E_{min}|$ is minimized with the appearance of a barrier-less ($\Delta E \sim k_B T$) potential profile for the moving ion. The dependence of ΔE on Q_f shown in (b) reveals the origin of the resonance-like behavior. In (c) for $Q_f = M0$, the self-potential barrier is balanced by electrostatic attraction to Q_f, resulting in a very low barrier with $1 \leq \Delta E \leq 2\, k_B T$.

Sodium ions exhibit a similar pattern but with $Q_{opt} = 0.45e$ (L0 band) providing valence selectivity between monovalent Na^{+} and divalent Ca^{2+} ions.

Multi-ion conduction is a consequence of the SF potential well becoming too deep (about $60k_B T$ for Ca^{2+} in the vicinity of M1), which makes the channel impermeable when occupied by a single ion. Conduction events then occur via a double-ion knock-on mechanism. The process is driven by the electrostatic interaction between simultaneously-captured ions, a mechanism that is especially effective for divalent Ca^{2+} ions [13], [9]. This barrier-less knock-on conductivity can be

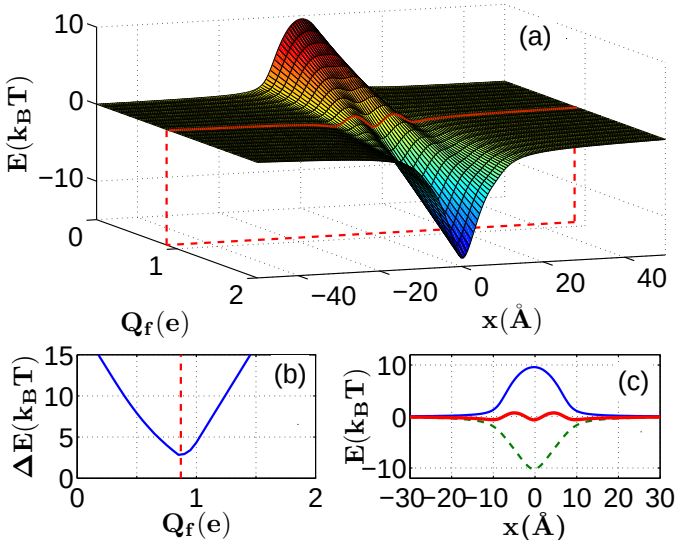

Fig. 3. The physical origin of the barrier-less conduction path for the channel M0. (a) The variation of electrostatic potential energy along the channel's $x-$axis is plotted as a function of the fixed charge Q_f. (b) The energy difference across the profile ΔE passes through a minimum at a particular value of $Q_f = Q_{opt}$ showing resonance-like behaviour. (c) The barrier-less energy profile (red) exists on account of a balance between the repulsion of the dielectric boundary force (blue) and the attraction to the fixed charge (green, dashed).

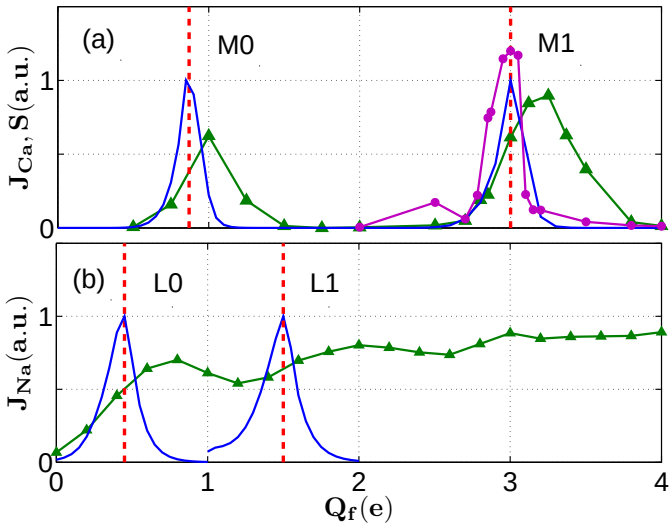

Fig. 4. Energetics and Brownian dynamics of the for single- and double-ion calcium and sodium bands. (d) The peaks in the calcium current J_{Ca} (green point-down triangles) and selectivity S (violet, circles) *vs.* Q_f calculated from electrostatics (blue curve) is in good agreement with the BD-simulated M0 and M1 peaks. (b) (b) The calculated peaks in the sodium current J_{Na} *vs.* Q_f is shifted down compared to the weak and overlapped conductance peaks L0, L1 (green point-down triangles) from BD simulations.

considered as a limiting case of long-range ion-ion correlations [14].

The coordinated movement of two interacting calcium or sodium ions can be described as the potential motion of the 2-ion entity ("super-ion") along an optimal stochastic trajectory (or minimum barrier height trajectory) on a 2D double-ion potential energy surface (PES) ([2], [10], [15]). This effectively reduces the problem to the case already discussed, i.e. the 1D movement of the super-ion in an electrostatic field resulting in very similar resonant dependence of ΔE on Q_f(see Fig. 3).

Fig. 4(a) presents a comparison between the calcium current J_{Ca} calculated from Kramers' approximation $J = J_0 \exp(-\Delta E/k_BT)$, and that obtained from the BD simulations for M0 and M1 (L-type channel) calcium bands. The reasonable agreement between the sharp current peaks confirms that the peaks of current in both M0 and M1 and selectivity S in the M1 band correspond to the points of barrier-less conductivity.

Fig. 4(b) presents a comparison between the sodium current J_{Na} calculated from Kramers' approximation, and that obtained from the BD simulations for L0 and L1 (Na_v sodium channel) sodium bands. The BD simulated maximum in the sodium current at $Q_{opt} = 2e$ is very weak, and is shifted up relative to the point of barrier-less conductance, due partly to kinetics effects (changes in the occupancy P vs Q_f), and partly to the obviously strong overlap between the different sodium bands.

V. Optimal double-ion trajectories

Fig. 5 presents Ca^{2+}-Ca^{2+} and Ca^{2+}-Na^{+} PES maps, optimal trajectories and corresponding energy profiles for Q_f=M1, at the point of maximum Ca^{2+}/Na^{+} selectivity. Fig. 5 (a),(b) shows the Ca^{2+}-Ca^{2+} PES map and the energy-optimal trajectory S, again navigating two deep orthogonal valleys. The almost flat energy profile along S (the energy difference along the optimal path ΔE does not exceed 1-2 k_BT) corresponds to fast barrier-less permeation. However, the heterogeneous Ca^{2+}-Na^{+} PES for M1 (Fig. 5(c),(d)) shows a high potential barrier $\Delta E \approx 20 k_BT$ impeding a sodium ion trying to knock-on a calcium ion. This barrier is unlikely to be overcome by thermal activation, implying deep blockade.

It is therefore clear that the calcium band M1 (L-type channel) corresponds to double-ion, resonance-like, barrier-less, conduction for Ca^{2+} ions, together with a deep blockade of Na^{+} ions, thereby resolving the selectivity *vs.* conductivity paradox for calcium channels.

The pattern for Na^{+}-Na^{+} permeation in the L1 band is rather similar but all effects are far less pronounced. Fig. 6 presents Na^{+}-Na^{+} and Ca^{2+}-Na^{+} PES maps, optimal trajectories, and the corresponding energy profiles for Q_f=L1 at the point of barrier-less conductivity. Plots (a),(b) show Na^{+}-Na^{+} PES map and energy optimal trajectory S corresponding to a knock-on event. S navigates two orthogonal valleys from South to East on the PES. The energy profile along S is almost flat (ΔE does not exceed $1 k_BT$) corresponding to fast, barrier-less, permeation. In contrast, the mixed Ca^{2+}-Na^{+} PES for L1 (Fig. 5(c),(d)) exhibits a high potential barrier ($\Delta E \approx 6 k_BT$) for a sodium ion trying to knock-on a calcium ion, which would need to be overcome by thermal activation, corresponded to calcium blockade in the DEKA sodium channel.

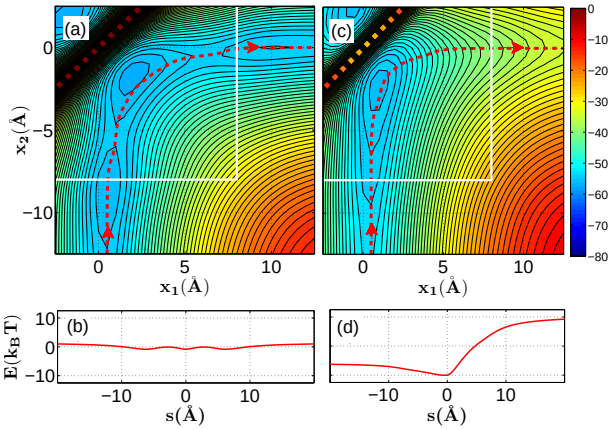

Fig. 5. Potential energy maps and profiles at Q_f corresponding to M1 for double-ion permeation. (a) The Ca^{2+}-Ca^{2+} PES map with superimposed optimal path S and (b) the corresponding potential energy E profile along S. The double-ion faces an almost barrier-less potential facilitating fast permeation. (c) The Ca^{2+}-Na^{+} energy map with optimal path S and (d) the corresponding potential energy E along S. The mixed super-ion needs to overcome a significant potential barrier, corresponding to divalent block. In the maps, the contour step is $1k_BT$, the optimal paths S are marked as dashed-red lines, and the selectivity filter boundary is shown by white lines. The direction of motion along S is shown by arrows.

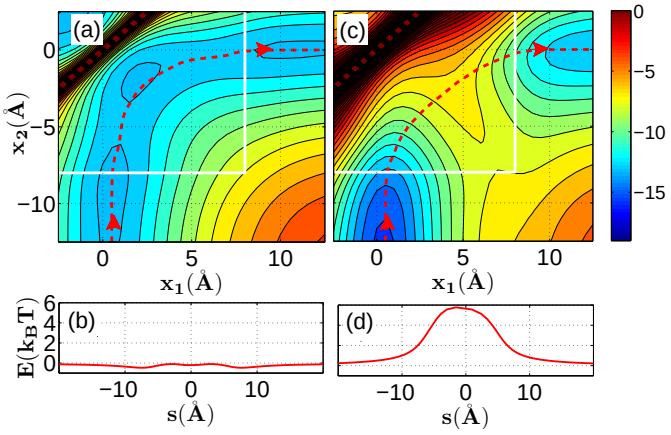

Fig. 6. Potential energy maps and profiles at Q_f corresponding to L1 for double-ion permeation. (a) The Na^{+}-Na^{+} energy map with superimposed optimal path S and (b) the corresponding potential energy E profile along S. The Na^{+}-Na^{+} double-ion faces an almost barrier-less ($\Delta E < k_BT$) potential profile facilitating fast permeation. (c) The Ca^{2+}-Na^{+} PES map with optimal path S and (d) the corresponding potential energy E profile along S. (d) The sodium ion needs to overcome a significant potential barrier (($\Delta E \approx 6k_BT$)), corresponding to divalent block. In the maps, the contour step is $1k_BT$, the optimal paths S are marked as dashed-red lines, and the selectivity filter boundary is shown by white lines. The direction of motion along S is shown by arrows.

VI. Conclusions

In summary, our Brownian dynamics simulations of ionic conduction within a generic model of a calcium-sodium channel for different values of the SF negative charge Q_f in the range $0-6.5e$ reveal an ordered sequence of selectivity bands with increasing calcium selectivity: L0$= 0.5-0.7e$ (sodium selective channel) $\rightarrow$ M0$= 1e$ (non-selective cation channel) $\rightarrow$ L1$= 1.5-2e$ (Na_v sodium channel) $\rightarrow$ M1$= 3e$ (L-type calcium channel) $\rightarrow$ M2$= 5e$ (RyR calcium channel).

Through the consideration of optimal trajectories on potential energy surfaces, we have shown explicitly that the conduction bands of the calcium/sodium channels arise as the result of single- and multi-ion barrier-less conduction. These resonance-like effects are much more pronounced for the divalent calcium bands M0 and M1.

Acknowledgements

The research was supported by the Engineering and Physical Sciences Research Council UK (grant No. EP/G070660/1).

References

[1] R. S. Eisenberg, "Interacting ions in biophysics: Real is not ideal," *Biophys J.*, vol. 104, no. 0, pp. 000–000, 2013.

[2] M. I. Dykman, P. V. E. McClintock, V. N. Smelyanskiy, N. D. Stein, and N. G. Stocks, "Optimal paths and the prehistory problem for large fluctuations in noise driven systems," *Phys. Rev. Lett.*, vol. 68, no. 18, pp. 2718–2721, 1992.

[3] B. Hille, *Ionic Channel Of Excitable Membranes*, 3rd ed. Sunderland, MA: Sinauer Associates, 2001.

[4] W. A. Sather and E. W. McCleskey, "Permeation and selectivity in calcium channels," *Ann. Rev. Physiol.*, vol. 65, pp. 133–159, 2003.

[5] E. Csányi, D. Boda, D. Gillespie, and T. Kristf, "Current and selectivity in a model sodium channel under physiological conditions: Dynamic Monte Carlo simulations," *Biochim. Biophys. Acta (BBA) – Biomembranes*, vol. 1818, no. 3, pp. 592–600, 2012.

[6] S. H. Heinemann, H. Teriau, W. Stuhmer, K. Imoto, and S. Numa, "Calcium-channel characteristics conferred on the sodium-channel by single mutations," *Nature*, vol. 356, no. 6368, pp. 441–443, 1992.

[7] T. Schlief, R. Schonherr, K. Imoto, and S. H. Heinemann, "Pore properties of rat brain II sodium channels mutated in the selectivity filter domain," *Eur. Biophys. J. & Biophys. Lett*, vol. 25, no. 2, pp. 75–91, 1996.

[8] I. Kaufman, D. G. Luchinsky, R. Tindjong, P. V. E. McClintock, and R. S. Eisenberg, "Multi-ion conduction bands in a simple model of calcium ion channels," *Phys. Biol.*, vol. 10, no. 2, p. 026007, 2013.

[9] B. Corry, T. W. Allen, S. Kuyucak, and S. H. Chung, "Mechanisms of permeation and selectivity in calcium channels," *Biophys. J.*, vol. 80, no. 1, pp. 195–214, 2001.

[10] V. N. Kharkyanen, S. O. Yesylevskyy, and N. M. Berezetskaya, "Approximation of super-ions for single-file diffusion of multiple ions through narrow pores," *Phys. Rev. E*, vol. 82, p. 051103, 2010.

[11] B. Nadler, T. Naeh, and Z. Schuss, "The stationary arrival process of independent diffusers from a continuum to an absorbing boundary is Poissonian," *SIAM J. Appl. Math.*, vol. 62, no. 2, pp. 433–447, 2001.

[12] I. Kaufman, D. G. Luchinsky, R. Tindjong, P. V. E. McClintock, and R. S. Eisenberg, "Energetics of discrete selectivity bands and mutation-induced transitions in the calcium-sodium ion channels family," *arXiv[physics.bio-ph]*, p. 1305.1847, 2013.

[13] P. Hess and R. W. Tsien, "Mechanism of ion permiation through calcium channels," *Nature*, vol. 309, no. 5967, pp. 453–456, 1984.

[14] R. Tindjong, I. Kaufman, P. V. E. McClintock, D. G. Luchinsky, and R. S. Eisenberg, "Nonequilibrium rate theory for conduction in open ion channels," *Fluct. Noise Lett.*, vol. 11, no. 1, p. 1240016, 2012.

[15] D. Gordon and S.-H. Chung, "Extension of Brownian dynamics for studying blockers of ion channels," *J. Phys. Chem. B*, vol. 116, no. 49, pp. 14 285–14 294, 2012.